Functional and Metabolomic Consequences of K_{ATP} Channel Inactivation in Human Islets

Changhong Li,[1,2] Amanda M. Ackermann,[1] Kara E. Boodhansingh,[1] Tricia R. Bhatti,[3] Chengyang Liu,[4] Jonathan Schug,[2] Nicolai Doliba,[2] Bing Han,[5] Karen E. Cosgrove,[5] Indraneel Banerjee,[5] Franz M. Matschinsky,[2] Itzhak Nissim,[6] Klaus H. Kaestner,[2,7] Ali Naji,[4] N. Scott Adzick,[8] Mark J. Dunne,[5] Charles A. Stanley,[1,2] and Diva D. De León[1,2]

Diabetes 2017;66:1901–1913 | https://doi.org/10.2337/db17-0029

Loss-of-function mutations of β-cell K_{ATP} channels cause the most severe form of congenital hyperinsulinism (K_{ATP}HI). K_{ATP}HI is characterized by fasting and protein-induced hypoglycemia that is unresponsive to medical therapy. For a better understanding of the pathophysiology of K_{ATP}HI, we examined cytosolic calcium ($[Ca^{2+}]_i$), insulin secretion, oxygen consumption, and [U-^{13}C]glucose metabolism in islets isolated from the pancreases of children with K_{ATP}HI who required pancreatectomy. Basal $[Ca^{2+}]_i$ and insulin secretion were higher in K_{ATP}HI islets compared with controls. Unlike controls, insulin secretion in K_{ATP}HI islets increased in response to amino acids but not to glucose. K_{ATP}HI islets have an increased basal rate of oxygen consumption and mitochondrial mass. [U-^{13}C]glucose metabolism showed a twofold increase in alanine levels and sixfold increase in ^{13}C enrichment of alanine in K_{ATP}HI islets, suggesting increased rates of glycolysis. K_{ATP}HI islets also exhibited increased serine/glycine and glutamine biosynthesis. In contrast, K_{ATP}HI islets had low γ-aminobutyric acid (GABA) levels and lacked ^{13}C incorporation into GABA in response to glucose stimulation. The expression of key genes involved in these metabolic pathways was significantly different in K_{ATP}HI β-cells compared with control, providing a mechanism for the observed changes. These findings demonstrate that the pathophysiology of K_{ATP}HI is complex, and they provide a framework for the identification of new potential therapeutic targets for this devastating condition.

Inactivating mutations of the two genes encoding the subunits of K_{ATP} channels expressed in pancreatic β-cells, *KCNJ11* and *ABCC8*, cause the most severe form of congenital hyperinsulinism (K_{ATP}HI) (1). In K_{ATP}HI, dysregulated insulin secretion results in a failure to suppress insulin secretion as plasma glucose concentrations decrease during fasting and a failure to increase insulin secretion in response to a glucose load (2). In contrast, a protein load inappropriately stimulates insulin secretion and results in protein-induced hypoglycemia (3). In most cases of K_{ATP}HI, medical therapy is not effective and pancreatectomy is required to control the hypoglycemia. For focal cases, resection of the lesion is curative; however, children with diffuse K_{ATP}HI may require a near-total pancreatectomy (4), which results in diabetes later in life (5,6).

The simplistic view of the pathophysiology of K_{ATP}HI, as understood today, is that lack of functional K_{ATP} channels leads to depolarized β-cells and elevation of cytosolic calcium

[1]Division of Endocrinology and Diabetes, Department of Pediatrics, The Children's Hospital of Philadelphia, Perelman School of Medicine, University of Pennsylvania, Philadelphia, PA
[2]Institute for Diabetes, Obesity, and Metabolism, Perelman School of Medicine, University of Pennsylvania, Philadelphia, PA
[3]Department of Pathology, The Children's Hospital of Philadelphia, Perelman School of Medicine, University of Pennsylvania, Philadelphia, PA
[4]Department of Surgery, Perelman School of Medicine, University of Pennsylvania, Philadelphia, PA
[5]Faculty of Biology, Medicine and Health, The University of Manchester, Manchester, U.K.
[6]Division of Metabolism, The Children's Hospital of Philadelphia, Perelman School of Medicine, University of Pennsylvania, Philadelphia, PA
[7]Department of Genetics, Perelman School of Medicine, University of Pennsylvania, Philadelphia, PA
[8]Department of Surgery, The Children's Hospital of Philadelphia, Perelman School of Medicine, University of Pennsylvania, Philadelphia, PA

Corresponding authors: Changhong Li, li@email.chop.edu, and Diva D. De León, deleon@email.chop.edu.

Received 6 January 2017 and accepted 15 April 2017.

This article contains Supplementary Data online at http://diabetes.diabetesjournals.org/lookup/suppl/doi:10.2337/db17-0029/-/DC1.

($[Ca^{2+}]_i$), which result in continuous insulin secretion, independent of plasma glucose concentration (7). While this explains some features of the clinical phenotype, such as the inability to turn off insulin secretion as glucose concentration decreases, it does not explain protein-induced hypoglycemia or impaired glucose responsiveness. We have shown in both mouse and human islets lacking functional K_{ATP} channels that there is a switch in fuel responsiveness from glucose to amino acids (8,9), which correlates with the protein-induced hypoglycemia observed clinically, but the mechanisms involved are not well understood. Data from studies in *Sur1*$^{-/-}$ mouse islets (8) and from a study of human K_{ATP}HI pancreas (10) suggest that elevated $[Ca^{2+}]_i$ is central to the increased responsiveness to amino acids.

While studies of K_{ATP} channel inactivation in mouse islets provide a foundation for understanding the pathophysiology of K_{ATP}HI, the molecular mechanisms leading to K_{ATP} channel inactivation in established mouse models differ from those in affected humans, and the phenotype of these mouse models is much milder than that observed in human patients (11–14). This indicates important limitations to the murine models and the importance of studying human islets. To examine stimulus-secretion coupling within the framework of the fuel metabolism/insulin secretion relationship in K_{ATP}HI, we have undertaken a comprehensive evaluation of the phenotype in islets isolated from the pancreases of children undergoing pancreatectomy for diffuse K_{ATP}HI.

RESEARCH DESIGN AND METHODS

Case Subjects

The diagnosis of hyperinsulinism was based on previously described criteria (15). Mutation analysis was performed by commercial laboratories. This study was approved by the institutional review board of The Children's Hospital of Philadelphia. Informed consent was obtained from all participants prior to inclusion in the study. Control human islets were obtained from the Integrated Islet Distribution Program (iidp.coh.org), and for some of the experiments, control islets isolated from the normal part of the pancreas of infants with focal HI were included for comparison.

Islet Isolation, Perifusion, and $[Ca^{2+}]_i$ Measurement

The procedure for islet isolation has previously been described (9). After 2–3 days of culture, islets were perifused with a ramp of amino acid mixture (AAM) (0–12 mmol/L) or with glucose (0–25 mmol/L) and exposed to 30 mmol/L KCl at the end of the perifusion. The AAM when used at maximum concentration of 12 mmol/L (~3 times physiological concentration) had the following composition (in mmol/L): glutamine 2.0, alanine 1.25, arginine 0.53, aspartate 0.11, citrulline 0.27, glutamate 0.35, glycine 0.85, histidine 0.22, isoleucine 0.27, leucine 0.46, lysine 1.06, methionine 0.14, ornithine 0.20, phenylalanine 0.23, proline 1.0, serine 1.62, threonine 0.77, tryptophan 0.21, and valine 0.57. For some of the perifusion experiments, 0.3 μmol/L glyburide was added to the perifusate. $[Ca^{2+}]_i$ responses were measured by dual-wavelength fluorescence microscopy with use of Fura-2 acetoxymethyl ester as previously described (16). Basal $[Ca^{2+}]_i$ was defined as the average $[Ca^{2+}]_i$ in the first 2 min of perifusion in absence of fuel after 30 min incubation with Fura-2 acetoxymethyl ester and 5 mmol/L glucose.

Stable Isotope Tracing, Intracellular Amino Acids, and ^{13}C Enrichment Assay

As previously described (16,17), 1,000 handpicked islets were preincubated with glucose-free Krebs-Ringer bicarbonate buffer (KRBB) for 30 min and then incubated with 4.0 mmol/L AAM with different concentrations of [U-^{13}C]glucose for 120 min. Insulin and glucagon concentrations in the supernatant were measured using the HTRF assay kit (Cisbio Bioassays, Bedford, MA). The intracellular amino acid profile was determined by high-performance liquid chromatography and ^{13}C enrichments were measured by gas chromatography–mass spectrometry as previously described (16,18).

mRNA Sequencing

β-Cells from isolated islets from two K_{ATP}HI case subjects (#20 and 21) and two normal infant control subjects were collected by FACS using the HIC1-2B4, HIC3-2D12, and HIC1-1C10 primary antibodies (a kind gift from Markus Grompe, Oregon Health Sciences University, Portland, Oregon) (19) and *R*-phycoerythrin–conjugated goat anti-mouse IgM and allophycocyanin-conjugated goat anti-mouse IgG secondary antibodies (Jackson ImmunoResearch Laboratories, West Grove, PA). Total RNA was collected using the Qiagen AllPrep DNA/RNA Micro Kit (category no. 80284) or Mini Kit (category no. 80204). RNA quality was determined using the Agilent 2100 Bioanalyzer; RNA integrity numbers were all >8. RNA sequencing (RNA-Seq) libraries were generated from 100 ng total RNA using the Illumina TruSeq Stranded Total RNA LT Sample Prep Kit (category no. RS-122-2301). Libraries were single-end sequenced to 100 bp on an Illumina HiSeq 2500 System. Raw sequenced reads were filtered to retain only high-quality reads, and ribosomal reads and repeats were eliminated. Remaining reads were processed with RNA-Seq Unified Mapper (RUM), which aligns reads to the set of known transcripts included in RefSeq, UCSC Genome Browser known genes, and Vega transcripts, and the genome, and outputs feature-level quantitation (transcript, exon, and intron). A total of 176–193 million reads mapped to the genome for each K_{ATP}HI case subject, while 36–48 million reads mapped to the genome for each control subject. For analysis of global gene expression profiles, the number of uniquely aligning reads to mRNA transcripts in RefSeq and UCSC genes were extracted from the RUM output. Pairwise comparisons between groups were carried using a custom script that implemented Bioconductor software's package edgeR to compute a *P* value and fold change for each transcript. The edgeR program adjusts for varying sequencing depths among samples. The data were summarized for individual genes by selection of a "representative transcript" with the highest read counts. The resulting *P* values were

corrected for multiple testing using the Benjamini and Hochberg mode of the R function p.adjust to compute a false discovery rate (FDR). Transcripts were considered significantly differentially expressed if the FDR was <0.05.

Immunohistochemistry

Paraffin-embedded pancreatic sections were immunolabeled as previously described (20). Primary antisera included anti-insulin (Invitrogen, Carlsbad, CA), anti-glucagon (Abcam, Cambridge, MA), and anti-Ki67 (BD Pharmingen, San Jose, CA), followed by incubation with secondary antisera conjugated to Cy2 or Cy3 (Jackson ImmunoResearch Laboratories). Nuclear staining was performed with DAPI (Molecular Probes, Eugene, OR). Morphometric analysis was performed as previously described (20). β- and α-Cell proliferation rate was determined as the percentage of insulin- or glucagon- and Ki67-positive cells over total insulin- or glucagon-positive cells, with at least 5,000 cells counted per case. β- and α-Cell areas were calculated as the percentage of the total pancreatic area containing islet cells positive for insulin and glucagon, respectively.

Oxygen Consumption, Transmission Electron Microscopy, and Serial Block Face-Scanning Electron Microscopy

Oxygen consumption in perifused islets was measured by a phosphorescence quenching method, using a new oxygen-sensitive phosphorescent porphyrin-dendrimer Oxyphor G3 (palladium-tetrabenzoporphyrin, encapsulated inside gen 2 poly-arylglycine dendrimer) as previously described (21–23). Tissue samples from control ($n = 3$) and K_{ATP}HI ($n = 3$) after surgery were fixed and processed for transmission electron microscopy (TEM) and serial block face-scanning electron microscopy using a high-contrast protocol as previously described (24,25). Raw data files were converted to an MRC (Medical Research Council, U.K.) file stack using IMOD software (Boulder, CA) (http://bio3d.colorado.edu/imod/), which was also used in three-dimensional reconstruction (24,25).

Calculations and Statistical Analyses

Glucose-derived ^{13}C enrichment of amino acids was expressed as molar percent enrichment, which is the molar fraction percent of analyte containing ^{13}C atoms above natural abundance, as previously described (17,26). All data are presented as means ± SE. Student *t* tests were used when two groups were compared. One-way ANOVA (GraphPad Prism) was used, followed by the Bonferroni test, when more than two groups were compared. Differences were considered significant when $P < 0.05$. For the RNA-Seq data, an FDR of <0.05 was considered significant.

RESULTS

Clinical and Genotype Information

We studied 21 case subjects with diazoxide-unresponsive congenital HI due to inactivating K_{ATP} channel mutations (K_{ATP}HI) who had diffuse disease suggested by genetic mutation analysis, preoperative 18-fluoro-L-3,4-dihydroxyphenylalanine positron emission tomography scan (1,27), and confirmed by histology. As shown in Table 1, 19 of 21 children had biallelic recessive mutations in the K_{ATP} channel genes (17 in *ABCC8* and 2 in *KCNJ11*), 1 of 21 had a monoallelic dominant *ABCC8* mutation (1,28), and 1 of 21 had a single monoallelic intronic variant in *ABCC8* of uncertain significance.

Alterations in Basal and Fuel-Stimulated Insulin Secretion

We examined fuel-stimulated insulin secretion in islets isolated from surgical pancreatic specimens and cultured for 2–3 days prior to perifusion. Control islets for the perifusion studies were obtained from cadaveric organ donors. Insulin content was significantly lower in K_{ATP}HI islets compared with control islets ($P < 0.001$), while glucagon content was not different (Fig. 1*A*). Basal insulin release was significantly higher in K_{ATP}HI islets compared with control islets ($P < 0.001$) (Fig. 1*B*). Glucose-stimulated insulin secretion (GSIS) was impaired in K_{ATP}HI islets, which were also not able to shut off insulin secretion when glucose was removed from the perifusate (Fig. 1*C* and *D*), while amino acid–stimulated insulin secretion (AASIS) was increased (Fig. 1*E* and *F*). This is in marked contrast to control islets that respond to stimulation with glucose (Fig. 1*C*) but had little or no response to stimulation with amino acids (Fig. 1*E*). Five additional cases showed a similar pattern of insulin secretion in perifusion protocol of AAM ramp followed by glucose ramp stimulation (Supplementary Fig. 1*A* and *B*). As expected, the K_{ATP} channel inhibitor glyburide stimulates insulin secretion in control islets but not in K_{ATP}HI islets (Fig. 1*G*). K_{ATP} channel inhibition with glyburide in control islets replicates the pattern of insulin secretion seen in K_{ATP}HI islets—higher basal insulin secretion, impaired GSIS, and enhanced AASIS (Fig. 1*H* and *I*)—demonstrating that the changes in basal and fuel-stimulated insulin secretion observed in K_{ATP}HI islets result from inactivation of the K_{ATP} channels. This pattern of fuel-stimulated insulin secretion is concordant with what we have previously reported in islets isolated from *Sur1*$^{-/-}$ mice (8) and explains the clinical observations from individuals with K_{ATP}HI, who have fasting hypoglycemia, impaired glucose tolerance, and protein-induced hypoglycemia (2,3). Surprisingly, islets from some case subjects (cases #13–16) showed a pattern of autonomous oscillatory insulin secretion regardless of secretagogue stimulation (Supplementary Fig. 1*C*). This phenomenon has not been described before in islets from *Sur1*$^{-/-}$ mice or from patients with K_{ATP}HI (8,10) but was previously seen in transgenic mouse islets expressing a constitutively active mutant version of glutamate dehydrogenase at very high levels (26).

Alterations in Basal and Stimulated $[Ca^{2+}]_i$ in K_{ATP}HI Islets

$[Ca^{2+}]_i$ in K_{ATP}HI and control islets was measured by dual-wavelength fluorescence microscopy using Fura-2 as a calcium indicator. Basal $[Ca^{2+}]_i$ was compared among islets from infants with diffuse K_{ATP}HI, control islets isolated from pancreatic tissue from the normal region of pancreas

Table 1—Subject information (all diffuse cases requiring 95–98% pancreatectomy)

Case	Gestational age (wks)	Birth weight (g)	Mutations (gene: paternal/maternal)	Max GIR (mg/kg/min)	Age at surgery (wks)	Outcome
1	34 2/7	4,420	ABCC8: p.Met80Arg/p.Leu511Pro	28	5	Persistent hypoglycemia
2	35 5/7	4,540	ABCC8: p.Gln954*/p.delGlu1209	25	4	Persistent hypoglycemia
3	39	3,145	ABCC8: p.Leu40Arg/p.Leu40Arg	8	20	Persistent hypoglycemia
4	39	3,790	ABCC8: c.2222+15 c>a/p.Arg598*	8	16	Persistent hypoglycemia
5	38 5/7	4,240	ABCC8: p.Arg1394Leu/p.Arg1394Leu	25	4	Persistent hypoglycemia
6	36 3/7	4,120	ABCC8: c.3992–9 g>a/c.3992–9 g>a	21	1.7	Persistent hypoglycemia
7	37	5,029	ABCC8: p.Arg1215Trp/p.Asp1472Asn	40	6	Persistent hypoglycemia
8	36 4/7	4,470	ABCC8: p.Asn188Ser/p.Arg837*	21.5	3	Persistent hypoglycemia
9	36	2,860	ABCC8: p.Ile1425Phe de novo/none	8	8	Persistent hypoglycemia
10	38 6/7	4,320	ABCC8: p.Pro1442Leu fs*19/c.1817+2 t>c	18.8	7	Persistent hypoglycemia
11	37	4,925	ABCC8: p.Ala355Thr and p.Arg1494Trp/c.2222+1 g>t	32.7	3	Persistent hypoglycemia
12	37	4,240	ABCC8: c.3992–9 g>a/c.3992–9 g>a	21	1.3	Hyperglycemia
13	37 3/7	4,048	ABCC8: c.2222+15 c>a/c.1933delG	18	4	Hyperglycemia
14	39	3,643	ABCC8: p.Glu501Lys/c.2041–21 g>a	17.5	8	Persistent hypoglycemia
15	36 5/7	4,300	KCNJ11: p.Arg136His/p.Arg136His	35	4	Hyperglycemia
16	36 2/7	5,000	ABCC8: p.Asp1472Asn/p.Tyr539*	26.7	3	Persistent hypoglycemia
17	39	4,006	ABCC8: none/c.3870+7 g>a	10.8	12	Euglycemic
18	38	3,310	ABCC8: p.delPhe1388/c3992–9 g>a	25.8	1.7	Persistent hypoglycemia
19	39	4,930	KCNJ11: p.Ala172Val/p.Ala172Val	8	7	Hyperglycemia
20	38 6/7	3,780	ABCC8: p.Arg837*(nonmaternal)/c.1732_ 1746dup15	15	8	Euglycemic
21	39 1/7	2,714	ABCC8: c.3992–9g>a/c.2117–1g>a	23	10	Hyperglycemia

GIR, glucose infusion rate; wks, weeks.

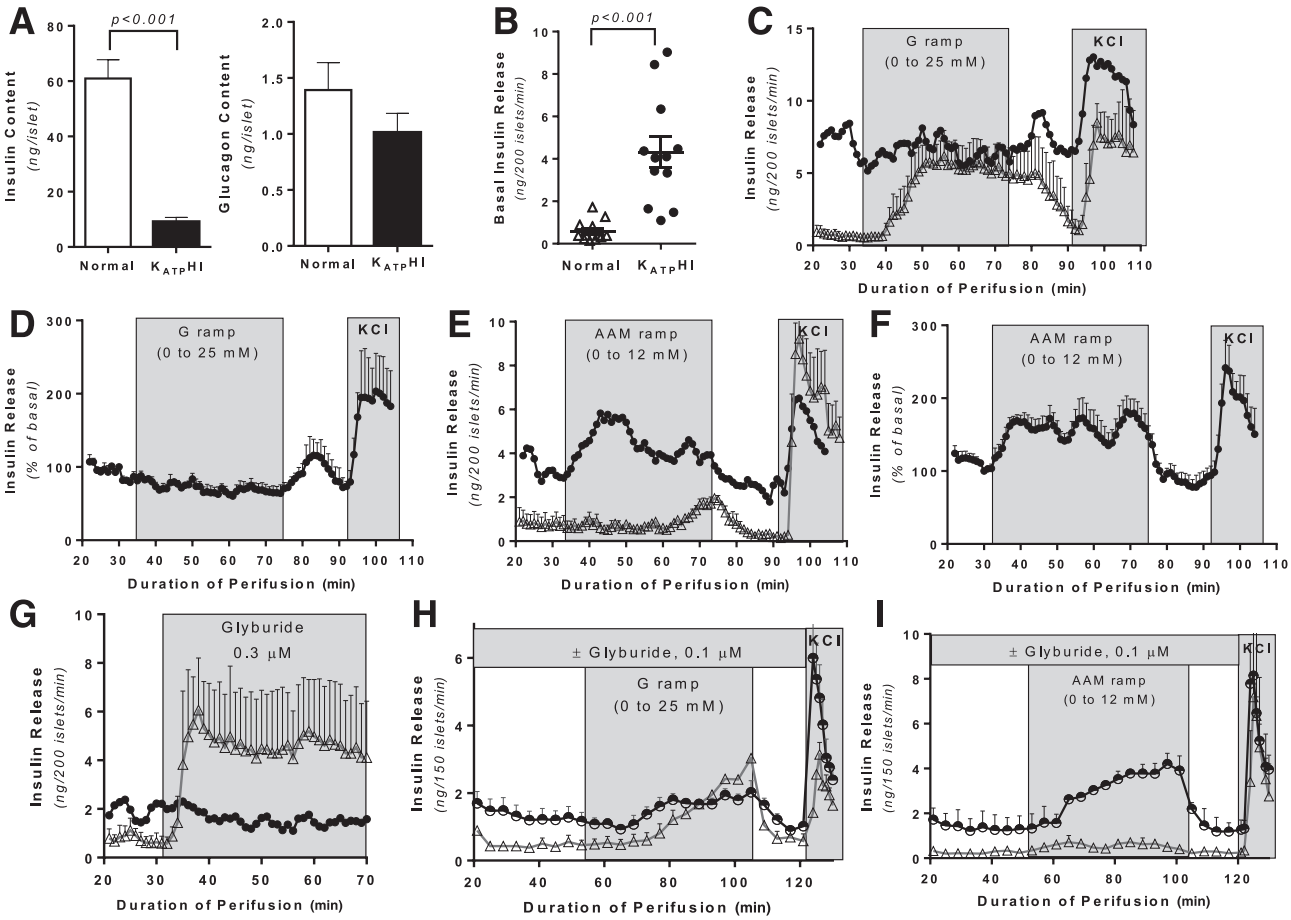

Figure 1—Insulin secretion in perifused islets isolated from K_{ATP}HI and control pancreas. After 2–3 days of culture, 200 islets were perifused with either an AAM or glucose and then exposed to 30 mmol/L potassium chloride. *A*: Insulin and glucagon content in control (n = 12) and K_{ATP}HI (n = 19) islets. *B*: Basal insulin release from control (n = 12) and K_{ATP}HI (n = 12) islets. *C*: GSIS (0–25 mmol/L with 0.625 mmol/L/min increment) in control (n = 3) and representative K_{ATP}HI (case #1) islets. *D*: GSIS (% from basal) in K_{ATP}HI islets (n = 5) (cases #1–5). *E*: AASIS (0–12 mmol/L with 0.3 mmol/L/min increment) in control (△) (n = 3) and representative K_{ATP}HI (●) (case #6) islets. *F*: AASIS (% from basal) in K_{ATP}HI islets (n = 6) (cases #1–6). *G*: Insulin secretion in response to glyburide (0.3 μmol/L) in control (△) (n = 3) and representative K_{ATP}HI (●) (case #1) islets. *H*: GSIS in the presence (half-filled circles) or absence (△) of glyburide (0.1 μmol/L) in control islets (n = 3 for each experimental condition). *I*: AASIS in the presence (half-filled circles) or absence (△) of glyburide (0.1 μmol/L) in control islets (n = 3 for each experimental condition). Data are mean ± SEM.

from age-matched infants with focal HI, and control islets isolated from adult cadaveric organ donors. Basal $[Ca^{2+}]_i$ was similar in the adult control islets and the islets from the normal region of pancreas from infants with focal HI. In contrast, basal $[Ca^{2+}]_i$ was significantly elevated in diffuse K_{ATP}HI islets compared with both the normal adult control islets and the age-matched control islets ($P < 0.01$) (Fig. 2*A*). Control islets, either from adult organ donors or from regions of normal pancreatic tissue from focal HI cases, showed calcium responses to both AAM and glucose (Fig. 2*B* and *C*). However, in K_{ATP}HI islets $[Ca^{2+}]_i$ increased slightly after AAM stimulation but did not change after glucose stimulation (Fig. 2*D*), in alignment with the observed insulin responses. We have previously shown that the $[Ca^{2+}]_i$ response to AAM in normal human islets correlated with release of glucagon but not insulin and therefore is likely to be from α-cells (16).

Increased Oxygen Consumption and Mitochondrial Mass in K_{ATP}HI Islets

In order to investigate the metabolic consequences of dysfunctional K_{ATP} channels, we measured oxygen consumption in K_{ATP}HI islets. As showed in Fig. 3, basal oxygen consumption rate (OCRs) in K_{ATP}HI islets was threefold higher than in control islets (0.74 ± 0.06 vs. 0.25 ± 0.01 nmol/min/100 islets; $P < 0.01$) (Fig. 3*A*), likely close to the maximum OCR, since neither AAM nor glucose further increased it (21) (Fig. 3*B* and *C*). The response to carbonilcyanide p-triflouromethoxyphenylhydrazone (FCCP) in K_{ATP}HI islets was normal, indicating that mitochondrial function is normal. Figure 3*D–F* shows a typical TEM plate of an HI β-cell and the localization of mitochondria within a secretory granule-rich region of the cell. For determination of the relative density of mitochondria within the control and HI β-cells, serial block face-scanning electron microscopy

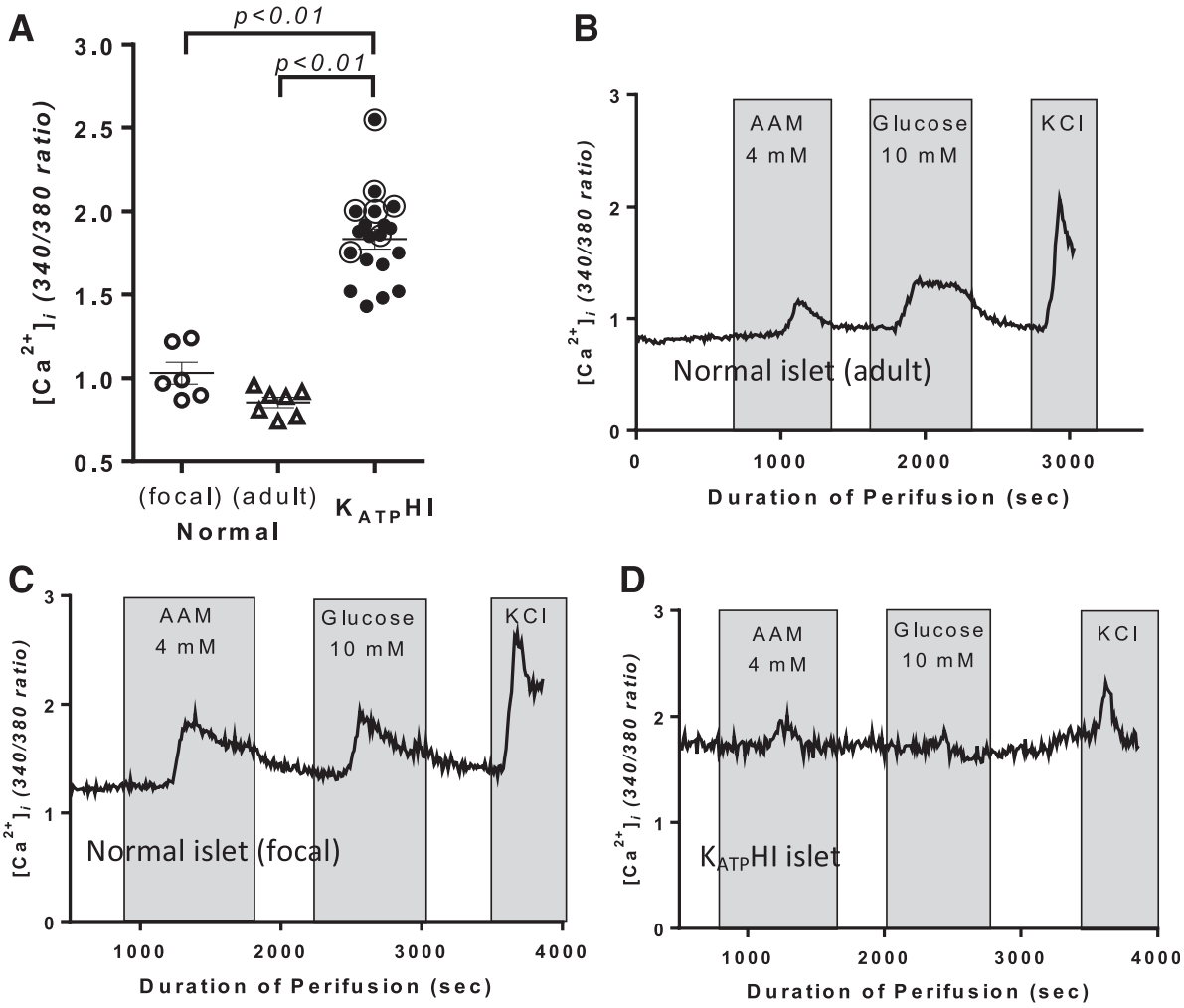

Figure 2—$[Ca^{2+}]_i$ dynamics in K_{ATP}HI and control islets. $[Ca^{2+}]_i$ dynamics were measured in isolated cultured islets using Fura-2 as calcium indicator. *A*: Basal $[Ca^{2+}]_i$ in control infant islets isolated from the normal pancreas region of focal cases (n = 6), control adult islets (n = 7), and K_{ATP}HI islets (n = 19). (Note: the circled cases were used for ^{13}C tracing experiments). *B–D*: $[Ca^{2+}]_i$ in adult control islets (*B*), age-matched infant control islets from normal pancreas region of focal HI (*C*), and K_{ATP}HI islets (*D*) in response to 4 mmol/L AAM and 10 mmol/L glucose stimulation, followed by 30 mmol/L KCl stimulation (representative cases are shown). sec, seconds.

was used to digitally reconstruct cells and their intracellular structures for volume measurements. This is made possible because high-resolution TEM images were generated in series from tissue samples of 100 nm thickness. In normal β-cells (n = 3), we found that the relative density of mitochondria was on average 2.88 ± 0.02% of the total cell volume (range 2.44–3.14) compared with 7.26 ± 0.03% in HI β-cells (n = 3) (range 6.70–8.32) ($P < 0.01$).

Alterations in Metabolism of [U-^{13}C]glucose in K_{ATP}HI Islets

We examined fuel metabolism in K_{ATP}HI islets (cases #7, #9, and #15–19) using a protocol to trace ^{13}C flux from [U-^{13}C]glucose in the presence of 4 mmol/L AAM as previously described (17). Control islets were cultured with 0.1 μmol/L glyburide for 3 days and during the experimental incubations to mimic K_{ATP}HI conditions. After 2 h incubation with different concentrations of [U-^{13}C]glucose (0, 5, and 25 mmol/L) and 4 mmol/L AAM, insulin and glucagon secretion and the concentrations and ^{13}C enrichments of intracellular amino acids were measured.

K_{ATP}HI Islets Have High Basal Insulin Secretion, Are Unresponsive to Glucose Stimulation, and Have Impaired Glucagon Secretion

Control islets without glyburide treatment showed robust insulin responses to 25 mmol/L glucose, with little response to 5 mmol/L glucose (Table 2). In contrast, control islets treated with glyburide responded similarly to K_{ATP}HI islets, with increased basal insulin secretion in the presence of AAM and impaired GSIS. K_{ATP}HI islets also had dramatically suppressed α-cell function: glucagon secretion was only 10% that of control islets, and glucose-mediated suppression of glucagon secretion was lost (Table 2). In contrast, 5 mmol/L glucose suppressed glucagon secretion by

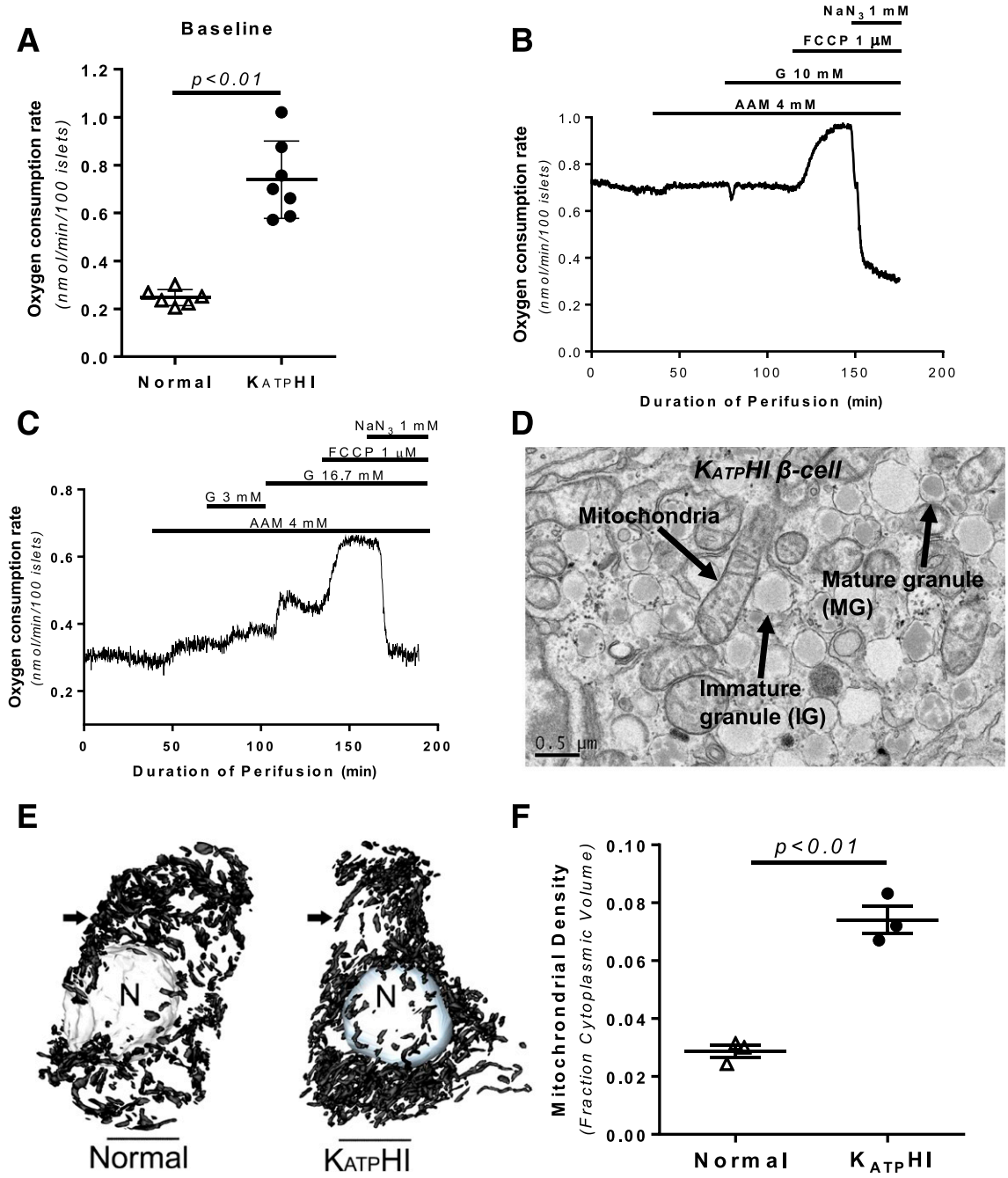

Figure 3—OCR and mitochondrial density in K_{ATP}HI and control islets. K_{ATP}HI and control islets were placed in respiratory chamber, and OCR was measured using phosphorescence quenching method as previously described (21). *A*: Basal OCR in control (n = 6) and K_{ATP}HI (n = 7) islets. *B*: OCR in K_{ATP}HI islets (n = 6) perifused with glucose-free KRBB and then exposed to 4.0 mmol/L AAM, 10 mmol/L glucose, 1 μmol/L FCCP, and 1 mmol/L NaN_3. *C*: OCR in control islets (n = 6) perifused with glucose-free KRBB and then exposed to 4.0 mmol/L AAM, 3 and 16.7 mmol/L glucose, and FCCP and then NaN_3. Note: *B* and *C* showed representative data, the signals were collected every 10 s, and for clarity we present typical experiments. *D–F*: Enhanced mitochondrial density in K_{ATP}HI β-cells. *D* shows the colocalization of mitochondria with secretory granules in a K_{ATP}HI β-cell, which are clearly identified by the presence of dense core/mature secretory granules and immature granular contents. Serial block face-scanning electron microscopy–derived digital reconstructions of β-cells from control and K_{ATP}HI tissue showing nuclear (N) and mitochondrial (arrow) structures (*E*) were used to determine relative mitochondrial densities evaluated (*F*) (n = 3 for control and K_{ATP}HI β-cells).

70% in control islets (Table 2). Control islets exposed to glyburide for 3 days showed normal basal glucagon secretion but had impaired glucose suppression of glucagon: 5 mmol/L glucose only suppressed glucagon secretion by 45%, partially reproducing the abnormal glucagon secretion in K_{ATP}HI islets.

Table 2—Insulin and glucagon secretion in K_{ATP}HI and normal human islets treated with glyburide

	Insulin secretion (μg/mg protein/2 h)			Glucagon secretion (pg/mg protein/2 h)		
	K_{ATP}HI (n = 7)	Normal + glyburide (n = 4)	Normal (n = 4)	K_{ATP}HI (n = 7)	Normal + glyburide (n = 4)	Normal (n = 4)
AAM 4.0/G 0	3.0 ± 1.0	4.3 ± 0.6	0.5 ± 0.1	11 ± 7	159 ± 34[A]	111 ± 34
AAM 4.0/G 5	3.2 ± 0.6	4.8 ± 0.7	0.8 ± 0.1	13 ± 8	89 ± 25[A]	31 ± 11[C]
AAM 4.0/G 25	2.6 ± 0.7	4.1 ± 0.9	3.4 ± 1.0	10 ± 6	61 ± 9[BC]	27 ± 9[C]

AAM 4.0, 4.0 mmol/L AAM; G 0, 0 mmol/L glucose; G 5, 5 mmol/L glucose; G 25, 25 mmol/L glucose. Versus K_{ATP}HI, [A]$P < 0.05$, [B]$P < 0.01$; vs. AAM 4.0/G 0, [C]$P < 0.05$.

K_{ATP}HI Islets Have High Rates of Glycolysis and Increased Serine/Glycine Biosynthesis

Compared with control islets and control islets treated with glyburide, total intracellular amino acid pools were not altered in K_{ATP}HI islets (Supplementary Table 1). However, glutamine and glycine concentrations were both significantly increased in K_{ATP}HI islets in glucose-free and 5 and 25 mmol/L glucose conditions. In addition, alanine concentration was more than twofold higher in K_{ATP}HI islets at 5 mmol/L glucose. In contrast, aspartate, γ-aminobutyric acid (GABA), and arginine were significantly lower in K_{ATP}HI islets. Arginine and isoleucine concentrations were reduced by 50% in K_{ATP}HI islets, but leucine levels were unchanged. Based on the intracellular amino acid concentrations and their ^{13}C enrichments (Supplementary Tables 1 and 2), we calculated the metabolic flux of ^{13}C from glucose to amino acids during the 2-h incubation period. The production of ^{13}C-alanine from [U-^{13}C]glucose was six times higher in K_{ATP}HI islets than in controls (Table 3). Thus, K_{ATP}HI islets have increased rates of glycolysis, since ^{13}C-alanine is produced via transamination from ^{13}C-pyruvate, which is derived from [U-^{13}C]glucose. This effect was not reproduced by 3 days' inhibition of K_{ATP} channel activity with glyburide treatment in control islets. In K_{ATP}HI islets, the M+2 ^{13}C labeling of alanine was twofold higher than M+3 labeling, whereas in control islets M+2 labeling was fourfold higher than M+3 labeling (Supplementary Table 2). A higher ratio of M+2 to M+3 alanine ^{13}C labeling in normal islets indicates a high rate of pyruvate cycling (17). The combination of high ^{13}C labeling of alanine and the reduced ratio of M+2 to M+3 in K_{ATP}HI islets indicates reduced rate of pyruvate cycling in K_{ATP}HI islets. K_{ATP}HI islets had markedly increased labeling of ^{13}C-serine and ^{13}C-glycine, while control islets or control islets pretreated with glyburide showed no ^{13}C flux into serine and glycine (Table 3), indicating that activation of the pathway for serine/glycine biosynthesis is unique to K_{ATP}HI islets.

K_{ATP}HI Islets Have Impaired GABA Shunt and Increased Glutamine Biosynthesis Activity

Compared with control islets and control islets treated with glyburide, intracellular aspartate was significantly lower in K_{ATP}HI islets (Supplementary Table 1), causing a 60% reduction in the production of ^{13}C-aspartate (Table 3). Because ^{13}C-asparate is produced from ^{13}C-oxaloacetate via transamination, the reduced ^{13}C-aspartate levels suggest that ^{13}C pool from glucose was diluted by unlabeled carbon sources in K_{ATP}HI islets. ^{13}C-glutamate production in K_{ATP}HI islets was slightly lower than in controls (both glyburide treated and untreated), but ^{13}C-GABA production was reduced by 90% in K_{ATP}HI islets (Table 3). This is consistent with our prior observations in *Sur1*$^{-/-}$ mouse islets, showing that inactivation of the K_{ATP} channels markedly impairs the activity of the GABA shunt (17). In contrast to impaired GABA shunt activity, K_{ATP}HI islets showed markedly increased production of ^{13}C-glutamine in comparison with control islets and control islets treated with glyburide.

Alterations in Gene Expression in K_{ATP}HI Islets

To investigate the molecular basis for the altered metabolism in K_{ATP}HI islets, we examined gene expression changes specifically in β-cells. We performed RNA-Seq on β-cells purified by FACS from two cases of K_{ATP}HI (cases #20

Table 3—Intracellular ^{13}C amino acid concentrations in K_{ATP}HI islets and normal islets with or without glyburide treatment

	AAM 4.0/G 5			AAM 4.0/G 25		
	K_{ATP}HI (n = 7)	Normal + glyburide (n = 4)	Normal (n = 4)	K_{ATP}HI (n = 7)	Normal + glyburide (n = 4)	Normal (n = 4)
^{13}C-alanine	20.5 ± 5.7	2.4 ± 1.2[A]	2.6 ± 1.8[A]	22.0 ± 8.0	3.6 ± 1.5[A]	4.1 ± 1.8[A]
^{13}C-aspartate	3.5 ± 1.9	15.5 ± 2.7[A]	11.7 ± 2.9[A]	3.1 ± 1.3	15.4 ± 2.2[A]	16.4 ± 5.2[B]
^{13}C-GABA	0.6 ± 0.2	8.9 ± 1.7[B]	9.6 ± 2.0[A]	0.4 ± 0.2	9.9 ± 1.1[B]	10.5 ± 1.7[B]
^{13}C-glutamate	41 ± 12	49 ± 11	67 ± 20	42 ± 15	72 ± 12	62 ± 13
^{13}C-glutamine	3.7 ± 1.0	0.8 ± 0.3[A]	1.0 ± 0.6[A]	4.8 ± 2.0	1.5 ± 0.7	1.2 ± 0.6
^{13}C-glycine/serine	3.2 ± 1.4	0	0	3.1 ± 1.6	0	0

AAM 4.0, 4.0 mmol/L AAM; G 5, 5 mmol/L glucose; G 25, 25 mmol/L glucose. Versus K_{ATP}HI, [A]$P < 0.05$, [B]$P < 0.01$.

and 21) and two sets of control islets from infants (3 and 6 months old). There were 3,890 genes upregulated and 3,022 genes downregulated in K_{ATP}HI β-cells compared with control β-cells (FDR <0.05). Expression of genes involved in the glycolysis, tricarboxylic acid cycle, and serine/glycine biosynthesis pathways in sorted β-cells are shown in Fig. 4*A*. Glycolytic pathway genes were significantly increased, consistent with the fuel metabolism findings reported above. The expression of hexokinase (*HK1*) was 16-fold higher in K_{ATP}HI β-cells, whereas glucokinase (*GCK*)

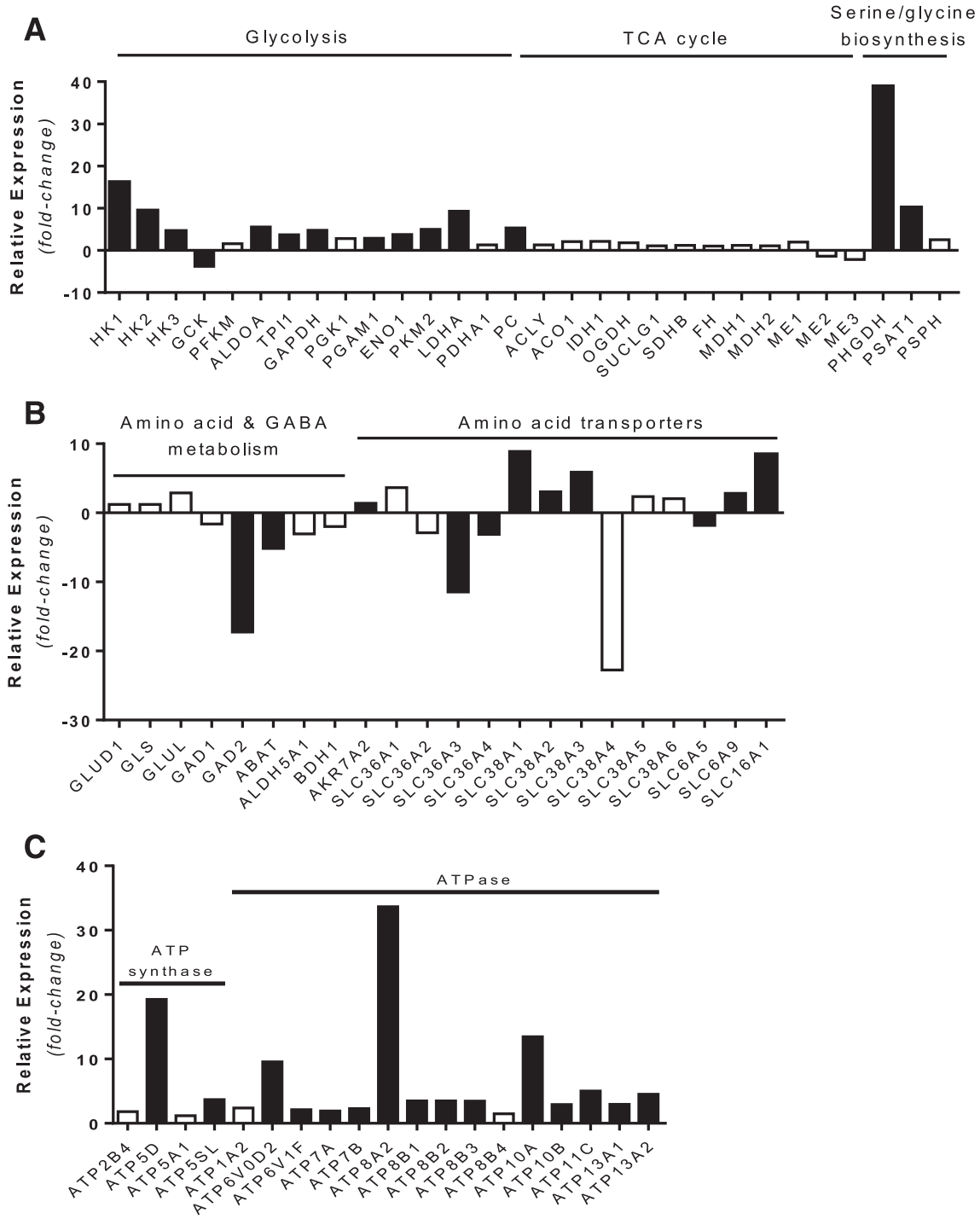

Figure 4—Gene expression in K_{ATP}HI and control β-cells. *A*: Relative expression of genes involved in glycolysis, tricarboxylic acid (TCA) cycle, and serine/glycine biosynthesis. *B*: Relative expression of genes involved in amino acid and GABA metabolism, as well as amino acid transporters. *C*: Relative expression of genes involved in ATP synthase and ATPase. Solid black bars represent genes expressed significantly different in K_{ATP}HI β-cells (FDR <0.001); open bars represent genes that were not expressed significantly different in K_{ATP}HI β-cells.

expression was dramatically reduced compared with control β-cells. The expression of other key glycolytic enzymes, phosphoglyceromutase 1 (*PGAM1*) and enolase (*ENO1*), was significantly increased as well. Expression of two key enzymes for serine/glycine biosynthesis, 3-phosphoglycerate dehydrogenase (*PHGDH*) and phosphoserine aminotransferase 1 (*PSAT1*), was increased by 38- and 10-fold, respectively, consistent with the isotopic labeling evidence of increased flux through this pathway (Fig. 4*A*). *GAD2* gene expression was significantly reduced along with GABA transaminase gene (ABAT) and succinate semialdehyde dehydrogenase gene (ALDH5A1), key steps of the GABA shunt, consistent with isotopic labeling evidence of decreased flux into GABA (Fig. 4*B*). In addition, there were also significant changes in the expression of amino acid transporters, as shown in Fig. 4*B*. In agreement with the observed high basal OCR and increased mitochondrial density in K_{ATP}HI islets, expression of ATP synthase and ATPase was significantly increased (Fig. 4*C*). These gene expression data suggest that K_{ATP}HI β-cells have a high rate of ATP production and consumption.

We also examined the RNA-Seq data for evidence of activation of the insulin or AMPK pathway. There is significant upregulation of *IRS1* transcript in the K_{ATP}HI β-cells compared with control β-cells, which may indicate that insulin signaling is elevated in K_{ATP}HI versus control β-cells. Similarly, the AMPK-α2 (*PRKAA2*), AMPK-γ2 (*PRKAG2*), and AMPK-γ3 (*PRKAG3*) subunit transcripts are downregulated in the K_{ATP}HI β-cells compared with control β-cells, which also suggest that insulin signaling is elevated in K_{ATP}HI versus control β-cells (data not shown).

Alterations in β-Cell Proliferation and β-Cell Area in K_{ATP}HI

To examine the effect of K_{ATP} channel inactivation on β- and α-cell proliferation and β- and α-cell areas, we counted the frequency of Ki67-positive nuclei among insulin- or glucagon-positive cells and measured β-cell and α-cell areas (as the percentage of the total pancreatic area containing islet cells positive for insulin and glucagon, respectively) in paraffin-embedded pancreatic tissue obtained from 40 case subjects with diffuse K_{ATP}HI (including the 21 described in Table 1) and 29 age-matched autopsy or surgical control subjects. The mean ages of K_{ATP}HI patients and of the age-matched control subjects were similar (6.0 ± 0.6 weeks, n = 40, vs. 7 ± 0.7 weeks, n = 29). We also obtained five autopsy or surgical control pancreatic tissue slides from older children (median age 4 years [range 10 months to 9 years]). β-Cell area in K_{ATP}HI subjects was significantly increased compared with that in age-matched control subjects ($P < 0.05$) (Fig. 5*A*). In contrast, α-cell area was slightly decreased in K_{ATP}HI pancreas (Fig. 5*B*), resulting in a 40% higher ratio of β-cell area versus α-cell area in K_{ATP}HI ($P < 0.01$) (Fig. 5*C*). The percentage of Ki67-positive cells among insulin-positive cells was significantly higher in K_{ATP}HI pancreas compared with that in pancreas of either age-matched or older control subjects ($P < 0.05$) (Fig. 5*D*). β-Cell proliferation rate was lower in older control subjects compared with 7-weeks-old control subjects, consistent with previous reports that β-cell proliferation normally declines with age (29,30).

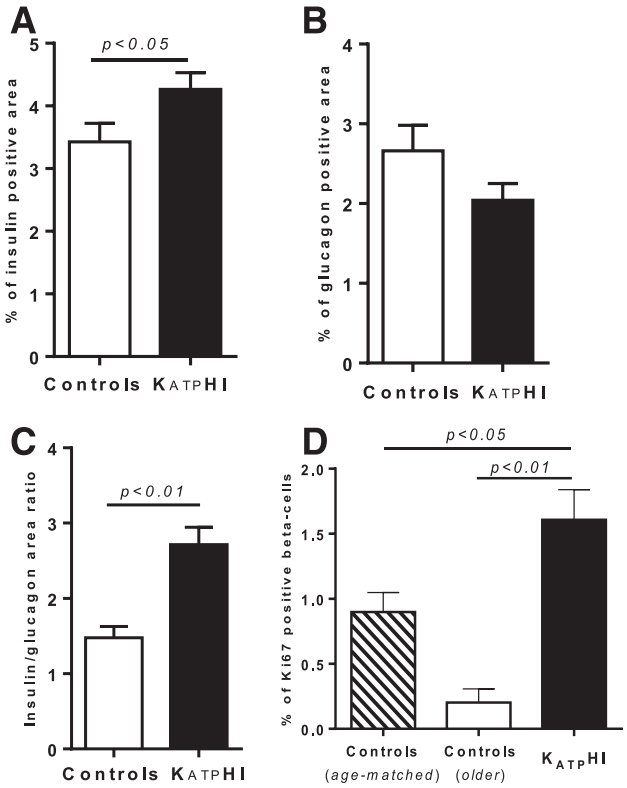

Figure 5—β/α-Cell mass and β-cell proliferation in pancreas from K_{ATP}HI and control infants. Pancreatic tissue slides were obtained from K_{ATP}HI, age-matched autopsy or surgical control subjects and older control subjects and immunolabeled for insulin, glucagon, and Ki67. *A*: β-Cell area as the percentage of the total pancreatic area containing islet cells positive for insulin among all cells in the slide in K_{ATP}HI (n = 40) and age-matched control (n = 29) subjects. *B*: α-Cell area as the percentage of the total pancreatic area containing islet cells positive for glucagon among all cells in the slide in K_{ATP}HI (n = 40) and age-matched control (n = 29) subjects. *C*: Ratio of β-cell to α-cell area in K_{ATP}HI (n = 40) and age-matched control (n = 29) subjects. *D*: Percentage of Ki67-positive cells among insulin-positive cells in K_{ATP}HI (n = 40), older control pancreata (n = 5), and age-matched control pancreata (n = 29).

DISCUSSION

Our studies of islets isolated from the pancreases of children undergoing pancreatectomy for K_{ATP}HI demonstrate cardinal features associated with loss of β-cell K_{ATP} channel activity that can partially explain the clinical phenotype. However, our data also reveal significant quantitative differences in β-cell gene expression and fuel metabolism in human K_{ATP}HI islets that are not replicated in normal human islets by acute blockade of K_{ATP} channels with glyburide and that are likely to play important roles in the pathophysiology of the disorder. K_{ATP}HI islets have elevated $[Ca^{2+}]_i$, leading to impaired insulin responses to glucose

stimulation and increased responses to amino acid stimulation, which are consistent with the effects of acute inhibition of β-cell K_{ATP} channels by glyburide in normal human islets. In addition, islets from K_{ATP}HI children also show altered glucose and amino acid metabolism, which are not replicated in glyburide-treated normal islets. The major features are as follows: increased glucose oxidation via glycolysis, increased glucose flux into the pathway for serine/glycine biosynthesis, and impaired oxidation of glutamate via the GABA shunt. These alterations in islet fuel metabolism correlate with changes in β-cell gene expression, including increased expression of *HK1* relative to *GCK*, increased expression of enzymes in the serine/glycine biosynthesis pathway, and decreased expression of *GAD2*, which mediates GABA production from glutamate.

Our islet studies demonstrate that the protein-induced hypoglycemia seen in children with K_{ATP}HI (3) is due to increased β-cell responsiveness to amino acids, explained, at least in part, by the elevated basal $[Ca^{2+}]_i$ levels (8,10). This fuel-sensing switch from glucose to amino acids in K_{ATP}HI islets may also reflect the alterations in amino acid metabolism demonstrated by our studies. Glutamine biosynthesis is increased in K_{ATP}HI islets, which may lead to downstream accentuation of an amplifying pathway, through glutamine signaling to induce amino acid–stimulated insulin release (8). In contrast to the increased ^{13}C flux to glutamine, GABA shunt activity is severely reduced in K_{ATP}HI islets. This decreased GABA shunt activity, which also occurs in human islets from individuals with type 2 diabetes (16,17), is explained by reduction of glutamate decarboxylase (*GAD*) gene expression, the key enzyme for GABA production.

An important feature of the phenotype of children with K_{ATP}HI is the observation that GSIS is impaired (2), which is clearly demonstrated in our experiments with isolated patient islets. This inappropriate β-cell response to glucose stimulation can be, at least in part, explained by alterations in the triggering pathway resulting from absence of K_{ATP} channel activity. However, additional mechanisms may also be involved in the altered responses to glucose, since the stable isotope ^{13}C tracer studies in K_{ATP}HI islets demonstrated marked increases in glycolysis. Upregulation of expression of *HK1* relative to *GCK*, which lowers the threshold for β-cell glucose metabolism and increases glycolytic flux, may explain this increased rate of glycolysis. Expression of the *HK1* gene, a low K_m hexokinase for glucose phosphorylation, is normally turned off after birth (31,32). Indeed, mutations in regulatory elements that cause increased *HK1* expression in β-cells have been linked to a novel form of hyperinsulinism (33). Along with increased glycolysis, serine/glycine biosynthesis was also enhanced in K_{ATP}HI islets. Increased expression of two key enzymes involved in serine/glycine biosynthesis, *PHGDH* and phosphoserine aminotransferase 1 (*PSAT1*), provides a mechanism for the enhanced serine/glycine biosynthesis. The serine/glycine biosynthesis pathway has been shown to be essential for the growth of certain cancer cells by providing material for nucleotide biosynthesis (34–36), and blocking this pathway limits cell division in cancer cells (35,37,38). Based on our immunohistochemistry studies, and as shown by others (39), β-cell proliferation is increased in K_{ATP}HI compared with age-matched control subjects. Previous studies have suggested that increased glycolysis due to glucokinase activation leads to increased β-cell proliferation in mice and humans (40,41). Thus, the activation of a serine/glycine biosynthesis pathway may play a key role in the linkage between glucose metabolism and β-cell proliferation in K_{ATP}HI.

Oxygen consumption showed greatly abnormal characteristics in K_{ATP}HI islets. Basal respiration was increased approximately threefold. Neither amino acids nor glucose stimulated the OCR, contrary to what is seen in perifused control islets. In addition, mitochondrial density was significantly increased in K_{ATP}HI islets in agreement with increased basal OCR. Two main questions require answers: what are the energy-consuming processes that drive the high rate of oxygen consumption, and what is (are) the endogenous fuel(s) that support(s) this high metabolic rate? It is probable that increased ion transport associated with the persistent membrane depolarization characteristic of β-cells of these case subjects augments ATP consumption, which cause the extreme OCR observed here, and that endogenous amino acids are the most likely substrate sustaining this high rate of oxidative metabolism, as suggested by the data of Supplementary Table 1. A low phosphate potential (ATP/ADP + P_i) would be the critical regulatory factor, resulting in the activation of glutamate dehydrogenase, which is involved in amino acid catabolism. In the presence of glucose, amino acid metabolism is reduced; yet, the total OCR does not change because energy demands of massively enhanced ion fluxes are not altered.

Intensive studies of the biochemical basis of glucose stimulation of insulin biosynthesis and secretion from the pancreatic β-cells have culminated in the widely accepted concept that increased metabolism of the stimulus and the ensuing alteration of metabolic coupling factor profiles (e.g., as most significant an increase of the ATP-to-ADP ratio) is the crucial event. This is possible only because the plasma glucose concentration determines the rate of glycolysis and oxidation in the β-cell by a "push mechanism" governed by the β-cell glucose sensor glucokinase, the hexose-phosphorylating enzyme with a substrate affinity constant in the range of basal glucose and lacking control by feedback. Availability of the nutrient thus drives intermediary metabolism including respiration and secretory function of the β-cell. This control of metabolism by push is the exception rather than the rule. In most other tissues, regulation of fuel metabolism is controlled by "pull mechanisms" governed by the energy requirements of the tissue. Isolated K_{ATP}HI islets have an abnormal, extremely high basal metabolic rate (e.g., ~3 times the control rate), which is not at all influenced by external fuel stimulants (e.g., amino acids or glucose). The most plausible explanation is that the constant membrane depolarization of K_{ATP}HI islets associated with increased ion influx and pumping (manifest by the

more than twofold elevation of intracellular calcium) augments ATP use greatly, which then initiates the use of endogenous fuel (most likely amino acids) through activating metabolic pathways controlled by the energy potential of the cell (ATP/ADP × P_i), characteristic for regulation by "pull mechanisms." The RNA-Seq data from sorted β-cells showing high *HEK*s1–3 and low *GCK* expression and the augmented mitochondrial mass per cell support this explanation. It seems that a persistently high calcium load and associated hypermetabolism results in a profound change of gene expression required to maintain the hypermetabolic state of K_{ATP}HI β-cells.

Certain methodological aspects of this study deserve consideration in interpreting the present results. Since islets were acquired from surgical specimens over several years, variations in the quality of the preparations may have affected results in individual case subjects. We assume that the case subjects selected for study all shared the same pathophysiology, since they had confirmed inactivating mutations of the K_{ATP} channel subunits. We did not detect any genotype-phenotype differences, but effects of differences in degree of channel defect or differences in genetic backgrounds remain possible. In addition, developmental changes might influence islet function in the patients, although experiments with "control" islets (normal tissue from focal HI) in a few cases did not show great differences between infants and adults with regard to intracellular calcium levels. The relative proportions of β-cell versus α-cell area were ~20% higher in K_{ATP}HI pancreas compared with controls; however, because the changes in the glucose tracer studies were >20%, the differences observed between patient, control, and glyburide-treated control islets are assumed to primarily reflect differences in β-cell metabolism, although this has not been confirmed by studies of individual types of islet cell.

In summary, our data provide novel insights into the pathophysiology of K_{ATP}HI in which chronic β-cell depolarization and elevation of $[Ca^{2+}]_i$ resulting from nonfunctional K_{ATP} channels lead to changes in gene expression and altered pathways of fuel metabolism and fuel responsiveness (Fig. 6). These secondary consequences of chronic plasma membrane depolarization may not be limited to K_{ATP}HI islets, since islets from individuals with type 2 diabetes share some characteristics of K_{ATP}HI islets, including increased expression of *HK1* and decreased expression of *GCK*, and impaired GABA shunt activity (16). We speculate that these patterns of gene expression and metabolic changes are largely the consequences of chronic or frequent depolarization and the accompanying persistent elevation of intracellular calcium. Our findings provide unique insights into the pathophysiology of K_{ATP}HI and shift the current paradigm that explains the pathophysiology of this devastating disease from an electrophysiological defect resulting solely in dysregulation of the triggering pathway of insulin secretion to a more complex picture, in which the primary K_{ATP} channel defect leads to secondary consequences affecting fuel metabolism and both the triggering and amplifying pathways of insulin secretion.

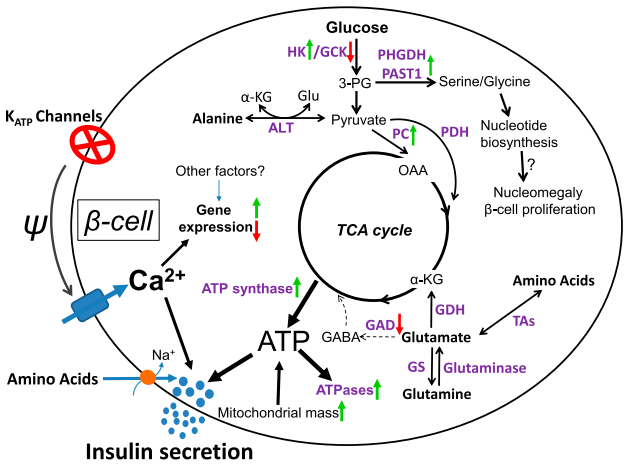

Figure 6—Diagram of K_{ATP}HI β-cell glucose and amino acid metabolism. In K_{ATP}HI, inactivating mutations of the β-cell K_{ATP} channels result in chronic β-cell depolarization and elevation of $[Ca^{2+}]_i$, which leads to alterations in fuel sensing and dramatic changes in fuel metabolism. Glycolysis is markedly increased, and the serine/glycine biosynthesis pathway is activated. The activation of a serine/glycine biosynthesis pathway may lead to increased nucleotide biosynthesis, β-cell nucleomegaly, and increased β-cell proliferation. K_{ATP}HI islets also have impaired GABA shunt and increased glutamine biosynthesis. Increased mitochondrial mass, oxygen consumption, and ATP synthase expression lead to high production of ATP. High rate of insulin release and increased expression of ATPases result in high ATP consumption. 3-PG, 3-phospoglycerate; α-KG, α-ketoglutarate; ALT, alanine transaminase; GDH, glutamate dehydrogenase; Glu, glutamate; GS, glutamine synthetase; OAA, oxaloacetate; PAST1, phosphoserine aminotransferase 1; PC, pyruvate carboxylase; PDH, pyruvate dehydrogenase; TAs, transaminases; TCA cycle, tricarboxylic acid cycle.

Acknowledgments. The authors thank Puja Patel, Pan Chen, and Stephanie Givler from the Division of Endocrinology and Diabetes, The Children's Hospital of Philadelphia, for their technical assistance.

Funding. This work was supported by National Institute of Diabetes and Digestive and Kidney Diseases (NIDDK), National Institutes of Health, grant 1R01-DK-098517-01A1 (to C.L. and D.D.D.L.), R37-DK-056268 (to C.A.S.), and University of Pennsylvania Diabetes Research Center National Institutes of Health grant P30-DK-19525. Human pancreatic islets were obtained through the NIDDK-funded Integrated Islet Distribution Program (http://iidp.coh.org/). Metabolome and fluxome profiling were performed by the The Children's Hospital of Pennsylvania metabolomic core.

Duality of Interest. No potential conflicts of interest relevant to this article were reported.

Author Contributions. C.L. designed and performed the experiments, analyzed data, and wrote the manuscript. A.M.A. performed RNA-Seq experiments and data analysis. K.E.B. and T.R.B. contributed to data collection. C.L. provided control normal islets. J.S. performed RNA-Seq experiments and data analysis. N.D. performed islet oxygen consumption experiments. B.H. performed the mitochondria density studies. K.E.C. performed the mitochondria density studies. I.B. contributed to data collection. F.M.M. contributed to data analysis and edited the manuscript. I.N. performed the metabolome and fluxome studies. K.H.K. contributed to data analysis and edited the manuscript. A.N. provided control normal islets and edited the manuscript. N.S.A. contributed to data collection and edited the manuscript. M.J.D. performed the mitochondria density studies and edited the manuscript. C.A.S. contributed to data analysis and edited the manuscript. D.D.D.L. designed the experiments, analyzed data, and edited the manuscript. C.L. and D.D.D.L. are the

guarantors of this work and, as such, had full access to all the data in the study and take responsibility for the integrity of the data and the accuracy of the data analysis.

Prior Presentation. Parts of this study were presented in abstract form at the 72nd Scientific Sessions of the American Diabetes Association, Philadelphia, PA, 8–12 June 2012.

References

1. Snider KE, Becker S, Boyajian L, et al. Genotype and phenotype correlations in 417 children with congenital hyperinsulinism. J Clin Endocrinol Metab 2013;98: E355–E363
2. Grimberg A, Ferry RJ Jr, Kelly A, et al. Dysregulation of insulin secretion in children with congenital hyperinsulinism due to sulfonylurea receptor mutations. Diabetes 2001;50:322–328
3. Fourtner SH, Stanley CA, Kelly A. Protein-sensitive hypoglycemia without leucine sensitivity in hyperinsulinism caused by K(ATP) channel mutations. J Pediatr 2006;149:47–52
4. Lord K, Dzata E, Snider KE, Gallagher PR, De León DD. Clinical presentation and management of children with diffuse and focal hyperinsulinism: a review of 223 cases. J Clin Endocrinol Metab 2013;98:E1786–E1789
5. Lord K, Radcliffe J, Gallagher PR, Adzick NS, Stanley CA, De León DD. High risk of diabetes and neurobehavioral deficits in individuals with surgically treated hyperinsulinism. J Clin Endocrinol Metab 2015;100:4133–4139
6. Beltrand J, Caquard M, Arnoux JB, et al. Glucose metabolism in 105 children and adolescents after pancreatectomy for congenital hyperinsulinism. Diabetes Care 2012;35:198–203
7. Kane C, Shepherd RM, Squires PE, et al. Loss of functional KATP channels in pancreatic beta-cells causes persistent hyperinsulinemic hypoglycemia of infancy. Nat Med 1996;2:1344–1347
8. Li C, Buettger C, Kwagh J, et al. A signaling role of glutamine in insulin secretion. J Biol Chem 2004;279:13393–13401
9. Calabria AC, Li C, Gallagher PR, Stanley CA, De León DD. GLP-1 receptor antagonist exendin-(9-39) elevates fasting blood glucose levels in congenital hyperinsulinism owing to inactivating mutations in the ATP-sensitive K+ channel. Diabetes 2012;61:2585–2591
10. Henquin JC, Nenquin M, Sempoux C, et al. In vitro insulin secretion by pancreatic tissue from infants with diazoxide-resistant congenital hyperinsulinism deviates from model predictions. J Clin Invest 2011;121:3932–3942
11. Miki T, Nagashima K, Tashiro F, et al. Defective insulin secretion and enhanced insulin action in KATP channel-deficient mice. Proc Natl Acad Sci U S A 1998;95: 10402–10406
12. Miki T, Tashiro F, Iwanaga T, et al. Abnormalities of pancreatic islets by targeted expression of a dominant-negative KATP channel. Proc Natl Acad Sci U S A 1997;94:11969–11973
13. Seghers V, Nakazaki M, DeMayo F, Aguilar-Bryan L, Bryan J. Sur1 knockout mice. A model for K(ATP) channel-independent regulation of insulin secretion. J Biol Chem 2000;275:9270–9277
14. Shiota C, Larsson O, Shelton KD, et al. Sulfonylurea receptor type 1 knock-out mice have intact feeding-stimulated insulin secretion despite marked impairment in their response to glucose. J Biol Chem 2002;277:37176–37183
15. Ferrara C, Patel P, Becker S, Stanley CA, Kelly A. Biomarkers of insulin for the diagnosis of hyperinsulinemic hypoglycemia in infants and children. J Pediatr 2016; 168:212–219
16. Li C, Liu C, Nissim I, et al. Regulation of glucagon secretion in normal and diabetic human islets by γ-hydroxybutyrate and glycine. J Biol Chem 2013;288: 3938–3951
17. Li C, Nissim I, Chen P, et al. Elimination of KATP channels in mouse islets results in elevated [U-^{13}C]glucose metabolism, glutaminolysis, and pyruvate cycling but a decreased gamma-aminobutyric acid shunt. J Biol Chem 2008;283:17238–17249
18. Li C, Najafi H, Daikhin Y, et al. Regulation of leucine-stimulated insulin secretion and glutamine metabolism in isolated rat islets. J Biol Chem 2003;278:2853–2858
19. Dorrell C, Abraham SL, Lanxon-Cookson KM, Canaday PS, Streeter PR, Grompe M. Isolation of major pancreatic cell types and long-term culture-initiating cells using novel human surface markers. Stem Cell Res (Amst) 2008;1:183–194
20. Teta M, Long SY, Wartschow LM, Rankin MM, Kushner JA. Very slow turnover of beta-cells in aged adult mice. Diabetes 2005;54:2557–2567
21. Doliba NM, Qin W, Najafi H, et al. Glucokinase activation repairs defective bioenergetics of islets of Langerhans isolated from type 2 diabetics. Am J Physiol Endocrinol Metab 2012;302:E87–E102
22. Doliba NM, Liu Q, Li C, et al. Accumulation of 3-hydroxytetradecenoic acid: cause or corollary of glucolipotoxic impairment of pancreatic β-cell bioenergetics? Mol Metab 2015;4:926–939
23. Lebedev AY, Cheprakov AV, Sakadzić S, Boas DA, Wilson DF, Vinogradov SA. Dendritic phosphorescent probes for oxygen imaging in biological systems. ACS Appl Mater Interfaces 2009;1:1292–1304
24. Han B, Newbould M, Batra G, et al. Enhanced islet cell nucleomegaly defines diffuse congenital hyperinsulinism in infancy but not other forms of the disease. Am J Clin Pathol 2016;145:757–768
25. Cross SE, Vaughan RH, Willcox AJ, et al. Key matrix proteins within the pancreatic islet basement membrane are differentially digested during human islet isolation. Am J Transplant 2017;17:451–461
26. Li C, Matter A, Kelly A, et al. Effects of a GTP-insensitive mutation of glutamate dehydrogenase on insulin secretion in transgenic mice. J Biol Chem 2006;281: 15064–15072
27. Hardy OT, Hernandez-Pampaloni M, Saffer JR, et al. Diagnosis and localization of focal congenital hyperinsulinism by ^{18}F-fluorodopa PET scan. J Pediatr 2007;150: 140–145
28. Yan FF, Lin YW, MacMullen C, Ganguly A, Stanley CA, Shyng SL. Congenital hyperinsulinism associated ABCC8 mutations that cause defective trafficking of ATP-sensitive K+ channels: identification and rescue. Diabetes 2007;56:2339–2348
29. Perl S, Kushner JA, Buchholz BA, et al. Significant human beta-cell turnover is limited to the first three decades of life as determined by in vivo thymidine analog incorporation and radiocarbon dating. J Clin Endocrinol Metab 2010;95:E234–E239
30. Wang YJ, Golson ML, Schug J, et al. Single-cell mass cytometry analysis of the human endocrine pancreas. Cell Metab 2016;24:616–626
31. Schuit F, Moens K, Heimberg H, Pipeleers D. Cellular origin of hexokinase in pancreatic islets. J Biol Chem 1999;274:32803–32809
32. Dhawan S, Tschen SI, Zeng C, et al. DNA methylation directs functional maturation of pancreatic β cells. J Clin Invest 2015;125:2851–2860
33. Pinney SE, Ganapathy K, Bradfield J, et al. Dominant form of congenital hyperinsulinism maps to HK1 region on 10q. Horm Res Paediatr 2013;80:18–27
34. Locasale JW, Cantley LC. Genetic selection for enhanced serine metabolism in cancer development. Cell Cycle 2011;10:3812–3813
35. Locasale JW, Grassian AR, Melman T, et al. Phosphoglycerate dehydrogenase diverts glycolytic flux and contributes to oncogenesis. Nat Genet 2011;43:869–874
36. Mullarky E, Mattaini KR, Vander Heiden MG, Cantley LC, Locasale JW. PHGDH amplification and altered glucose metabolism in human melanoma. Pigment Cell Melanoma Res 2011;24:1112–1115
37. Possemato R, Marks KM, Shaul YD, et al. Functional genomics reveal that the serine synthesis pathway is essential in breast cancer. Nature 2011;476:346–350
38. Jones NP, Schulze A. Targeting cancer metabolism–aiming at a tumour's sweet-spot. Drug Discov Today 2012;17:232–241
39. Kassem SA, Ariel I, Thornton PS, Scheimberg I, Glaser B. Beta-cell proliferation and apoptosis in the developing normal human pancreas and in hyperinsulinism of infancy. Diabetes 2000;49:1325–1333
40. Dadon D, Tornovsky-Babaey S, Furth-Lavi J, et al. Glucose metabolism: key endogenous regulator of β-cell replication and survival. Diabetes Obes Metab 2012; 14(Suppl. 3):101–108
41. Kassem SA, Ariel I, Thornton PS, et al. p57(KIP2) expression in normal islet cells and in hyperinsulinism of infancy. Diabetes 2001;50:2763–2769